Available online at www.sciencedirect.com
SCIENCE DIRECT®

Journal of the European Ceramic Society 23 (2003) 2031–2037

www.elsevier.com/locate/jeurceramsoc

Weibull analysis of ceramics under high stress gradients

T. Fett[a,*], E. Ernst[a], D. Munz[a], D. Badenheim[b], R. Oberacker[b]

[a]*Forschungszentrum Karlsruhe, Institut für Materialforschung II, Postfach 3640, 76021 Karlsruhe, Germany*
[b]*Universität Karlsruhe, Institut für Keramik im Maschinenbau, 76021 Karlsruhe, Germany*

Received 6 July 2002; received in revised form 9 December 2002; accepted 15 December 2002

Abstract

The Weibull parameter m of the strength distribution of ceramics under high stress gradients differs from that for moderate stress gradients. This is shown for contact loading. Bars were loaded by oppositely concentrated forcers via rollers. For most investigated materials, measured contact strengths showed strongly reduced Weibull exponents compared with those from 4-point bending tests. This was the reason for a study, in which the effective volumes and surfaces for the two tests were compared and the influence of the strong stress gradients was considered. Under the assumption of the Weibull theory being valid, the effective surfaces and volumes were computed for the normal stress and the energy release rate criteria. In the second part, it will be shown that the strongly non-homogeneous stresses lead to a reduced Weibull exponent.

Keywords: Mechanical properties; Strength; Stress gradients; Weibull modulus

1. Introduction

Ceramic materials fail by the unstable extension of flaws. The flaw size distribution is responsible for the large scatter of these materials and for effect of the size of a component on the strength.[1–3] The effect of a multiaxial stress distribution in a component on the strength distribution is described by the multiaxial Weibull theory.[4–6] The failure probability is given by the relation

$$F = 1 - \exp\left[-\left(\frac{\sigma_c}{\sigma_0}\right)^m\right] \quad (1)$$

σ_c is the critical value of a characteristic stress. The Weibull parameter m depends on the material, whereas σ_0 depends on the material and in addition on the multiaxial stress distribution in the component. For a detailed description see Ref. 7. The assumption for this theory is a constant stress along the flaw. For moderate stress gradients this assumption is fulfilled approximately. For large stress gradients as in contact loading this assumption is not valid and m depends on the stress distribution.[8]

In Ref. 9 a test was developed for the determination of strength under contact loading. Whereas conventional strength tests describe the failure behaviour of materials under simple stress states which, in most cases, comprise uniaxial stresses with relatively small stress gradients, the strength behaviour under strongly non-homogeneous and multiaxial stress states is measured in the test presented here.

The contact strength test proposed in Ref. 9 is illustrated in Fig. 1. Two cylinders of 8 mm diameter made of hardened steel are pressed onto the rectangular specimen with a force P.

In Fig. 2 the Weibull parameters for several ceramics are compiled. In this representation the rectangles represent the 90% confidence intervals. The commercial alumina investigated were: V38, CeramTec, Plochingen (an alumina containing about 4 wt.% glass phase), EKasic F (SiC), Wacker Ceramics, Kempten, Frialit F99.7 ($d_m \approx 9$ μm), and Frialit F99.9 ($d_m \approx 2.3$ μm) both from Friatec, Friedrichsfeld. Frialit F99.7 was tested in two different surface states characterised by the following surface roughness data: material F99.7(I) Ra = 0.7 μm, Rpk = 0.3 μm, Rk = 1.6 μm, Rvk = 1.7 μm, material F99.7(II) Ra = 1.0 μm, Rpk = 0.4 μm, Rk = 2.0 μm, Rvk = 2.2 μm. The other materials were a fine-grained AlN (CeramTec,

* Corresponding author. Tel.: +49-7247-82-2347; fax: +49-7247-82-5070.
E-mail address: theo.fett@imf.fzk.de (T. Fett).

0955-2219/03/$ - see front matter © 2003 Elsevier Science Ltd. All rights reserved.
doi:10.1016/S0955-2219(03)00024-4

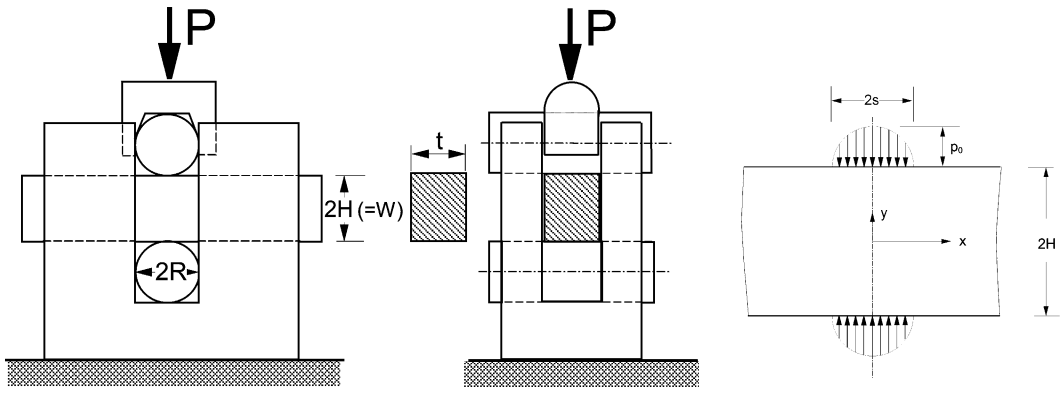

Fig. 1. A two-roller test device for contact strength tests and Hertzian pressure distribution.

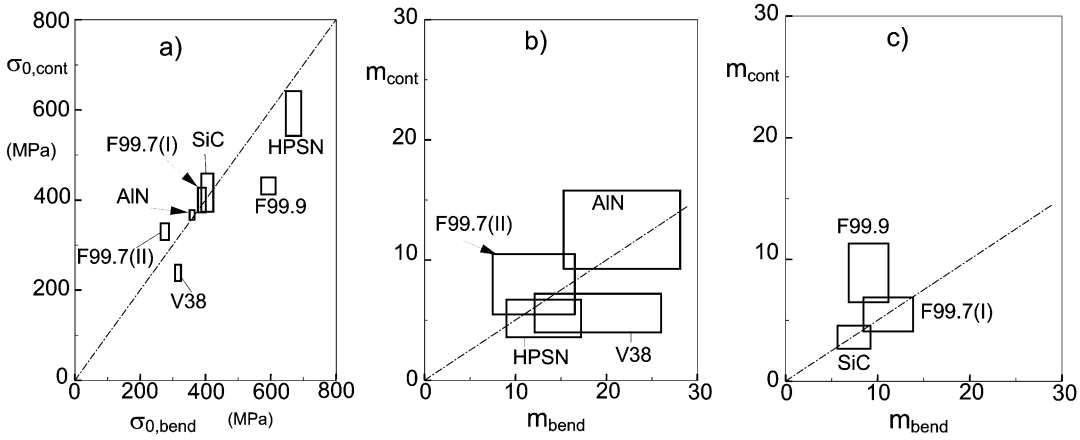

Fig. 2. Interrelation between Weibull parameters of contact strength and four-point bending strength tests: (a) characteristic strength σ_0, (b) and (c) Weibull exponent m (widths and heights of rectangles given by the 90% confidence intervals).

Marktredwitz) and a low-strength HPSN (NH209, Annawerk, Rödental).

The experiments on these ceramics yielded[8,9]

- a linear relation between the Weibull parameters σ_0 for bending strength and contact strength with roughly

  $\sigma_{0,\,\mathrm{bend}} \approx \sigma_{0,\,\mathrm{cont}}$

  as shown in Fig. 2a, where the 90% confidence intervals for the two tests are plotted,
- and lower Weibull exponents in the roller tests compared to the four-point bending tests as shown in Fig. 2b and c by the 90% confidence intervals for the second Weibull parameter m. The only exception was found for the fine-grained Al_2O_3 (Frialit F 99.9). This material showed identical Weibull exponents in bending and contact loading.

From microscopic observation of fracture surfaces, it can be concluded that failure starts from surface flaws. In a recent paper, it could be shown that for cracks extending directly at the end of the Hertzian contact zone, the effective stress intensity factor depends linearly on the crack size. This behaviour results in reduced Weibull exponents for the strength.[8] In the present investigation, a more detailed analysis will be given.

2. Stresses for opposed loads

For contact between the cylinders and the plane bar, the pressure distribution acting over the region $-s \leqslant x \leqslant s$ is

$$p(x) = p_0\sqrt{1-(x/s)^2}, \quad p_0 = \frac{2P}{s\pi t} \tag{2}$$

with the maximum pressure p_0 related to the total force P (Fig. 1). Under this load, the failure relevant stress components are[9]

$$\sigma_x = -2p_0\int_0^\infty \frac{1}{u}\frac{\sinh u - u\cosh u}{\sinh 2u + 2u}\cos\frac{ux}{H}J_1(us/H)\cosh\frac{uy}{H}\,\mathrm{d}u - 2p_0\int_0^\infty \frac{y}{H}\frac{\sinh u}{\sinh 2u + 2u}\cos\frac{ux}{H}J_1(us/H)\sinh\frac{uy}{H}\,\mathrm{d}u \tag{3}$$

$$\tau_{xy} = 2p_0\int_0^\infty \frac{1}{u}\frac{u\cosh u}{\sinh 2u + 2u}\sin\frac{ux}{H}J_1(us/H)\sinh\frac{uy}{H}\,\mathrm{d}u - 2p_0\int_0^\infty \frac{y}{H}\frac{\sinh u}{\sinh 2u + 2u}\sin\frac{ux}{H}J_1(us/H)\cosh\frac{uy}{H}\,\mathrm{d}u \tag{4}$$

with the Bessel function of first order, J_1. The maximum tensile stress in the bar is reached at the upper and lower surfaces, $y = \pm H$, directly beside the rollers ($x \approx 0$). At these locations

$$\sigma_{\max} = 0.490\frac{P}{Ht} \tag{5}$$

3. Conventional Weibull evaluation

In a first fracture mechanics evaluation, the Weibull method is applied. It ignores the strong stress gradients in the contact region. The equivalent stress σ_{eq} representing the multiaxial stress state can be written as the product of the maximum principal stress σ_1 and a function h

$$\sigma_{\mathrm{eq}} = \sigma_1\, h(\alpha, \gamma) \tag{6}$$

where $\alpha = \sigma_2/\sigma_1$ describes the multiaxiality and γ is the angle between the maximum principal stress and the crack normal (see e.g. Ref. 7). The special function h depends on the choice of the local failure criterion. In the following considerations, surface cracks under plane stress conditions are assumed only.

The maximum principal stress varying with the location in the component can be expressed by a reference stress σ^* (e.g. the maximum principal stress in the component) and a geometric function

$$\sigma_1 = \sigma^*\, g(x, y, z). \tag{7}$$

The failure probability under multiaxial loading is

$$F = 1 - \exp\left[-\frac{S_{\mathrm{eff}}}{S_0}\left(\frac{\sigma^*}{\sigma_0}\right)^m\right] \tag{8}$$

with the effective surface S_{eff} computed by

$$S_{\mathrm{eff}} = \frac{1}{2\pi}\int_{(S)} g^m\left[\int_0^{2\pi} h^m\,\mathrm{d}\gamma\right]\mathrm{d}S \tag{9}$$

(integration carried out over positive σ_1). In the following sections, only uniaxial and biaxial stress states are considered. In the special case of a uniaxial stress ($\alpha = 0$), h is constant and Eq. (9) simplifies to

$$S_{\mathrm{eff}} = \frac{1}{2\pi}\int_0^{2\pi} h^m\,\mathrm{d}\gamma\int_{(S)} g^m\,\mathrm{d}S \tag{10a}$$

In this case, the ratio of the effective surfaces for two different specimens (subscripts 1 and 2) is given by

$$S_{\mathrm{eff},1}/S_{\mathrm{eff},2} = \int_{S_1} g_1^m\,\mathrm{d}S \Big/ \int_{S_2} g_2^m\,\mathrm{d}S \tag{10b}$$

independently of the special failure criterion.

3.1. Normal stress criterion

As an appropriate failure criterion for natural cracks, the normal stress criterion is considered. For uniaxial stresses ($\alpha = 0$)

$$\sigma_{\mathrm{eq}} = \sigma_1\cos^2\gamma, \quad h = \cos^2\gamma \tag{11}$$

it results

$$S_{\mathrm{eff}} = \frac{1}{\sqrt{\pi}}\frac{\Gamma(m+\frac{1}{2})}{\Gamma(m+1)}\int_{(S)} g^m\,\mathrm{d}S \tag{12}$$

For the special case of a *four-point bending* bar with an inner loading span L and thickness B, we obtain

$$S_{\mathrm{eff,4PB}} = \frac{1}{\sqrt{\pi}}\frac{\Gamma(m+\frac{1}{2})}{\Gamma(m+1)}BL \tag{13}$$

The effective surface for the contact loading test was determined numerically at the surface stresses shown in Fig. 3a. The results are expressed as

$$S_{\mathrm{eff,cont}} = \lambda\frac{\Gamma(m+\frac{1}{2})}{\sqrt{\pi}\Gamma(m+1)}BW \tag{14}$$

with the coefficient λ plotted in Fig. 3b. An approximation of this coefficient reads

$$\lambda \cong \frac{2}{\sqrt{m}} \tag{15}$$

The ratio between the contact strength and the four-point bending strength results from (8) and (10b)

$$\frac{\sigma_{\mathrm{cont}}}{\sigma_{\mathrm{4PB}}} = \left(\frac{S_{\mathrm{eff,4PB}}}{S_{\mathrm{eff,cont}}}\right)^{1/m} = \left(\frac{L}{\lambda W}\right)^{1/m} \cong \left(\frac{\sqrt{m}L}{2W}\right)^{1/m} \tag{16}$$

3.2. Energy release rate criterion

Under loading by normal and shear stresses (σ_{n}, τ), an equivalent stress based on the complanar energy release rate criterion reads

$$\sigma_{\mathrm{eq}} = \sqrt{\sigma^2 + k\tau^2} \tag{17}$$

In the *uniaxial loading* case, it holds for the special case $k = 1$ that

$$\sigma_{\mathrm{eq}} = \sigma_1\cos\gamma \tag{18}$$

and therefrom the effective surface results as

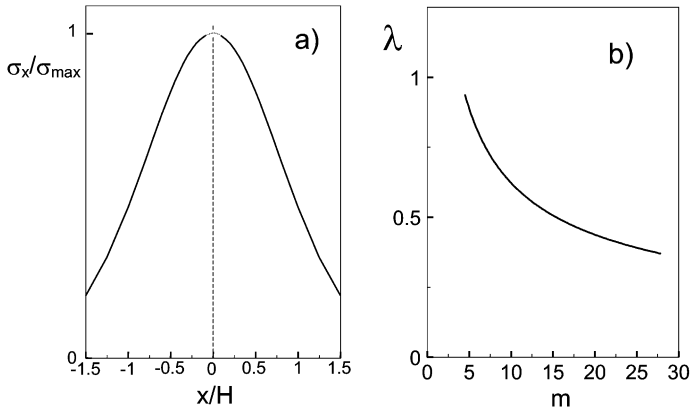

Fig. 3. (a) Axial stress along the free surface of a bar under cylinder contact loading, (b) coefficient λ defined by Eq. (14) as a function of m.

$$S_{\text{eff}} = \frac{1}{\sqrt{\pi}} \frac{\Gamma(\frac{m+1}{2})}{\Gamma(\frac{m}{2}+1)} \int_{(S)} g^m \mathrm{d}S \tag{19}$$

and

$$S_{\text{eff,4PB}} = \frac{1}{\sqrt{\pi}} \frac{\Gamma(\frac{m+1}{2})}{\Gamma(\frac{m}{2}+1)} BL \tag{20}$$

$$S_{\text{eff,cont}} = \lambda \frac{1}{\sqrt{\pi}} \frac{\Gamma(\frac{m+1}{2})}{\Gamma(\frac{m}{2}+1)} BW \tag{21}$$

Eq. (16) is valid also in the case of the energy release rate criterion. With the usual specimen data $L = 20$ mm, $W = 3$ mm, it results for $m = 10$: $\sigma_{\text{cont}} = 1.26\sigma_{\text{4PB}}$. Such a higher contact strength is not found by the experiments (Fig. 2a). Moreover, the Weibull exponents have to be identical for both tests. Also this result cannot be seen in the experiments.

4. Single surface cracks

In conventional Weibull theory, the stresses in a component are assumed to be constant over the crack dimensions. This assumption is always fulfilled for bending tests, but violated in a contact strength test near the loading cylinders. In order to include the strong stress gradients into the failure analysis, single natural cracks shall now be considered (modelled as edge cracks).

The stress state in a bar under contact loading by cylinders may be demonstrated here for the case of $s/H = 0.1$. The stress components σ_x and τ_{xy} are plotted in Fig. 4 over the cross-section of the bar under contact loading. The stress component σ_x is positive only in a very thin surface layer and then changes to compression. The shear stress τ_{xy} is zero at the free surface and increases very strongly with increasing depth. The smaller the distance from the contact area is, the steeper are the stress gradients.

From the stresses present in the uncracked body, the stress intensity factors K_{I} and K_{II} can be computed according to

$$K_{\text{I}} = \int_0^a h_{\text{I}}(\eta, a)\sigma_x(\eta)\mathrm{d}\eta \tag{22}$$

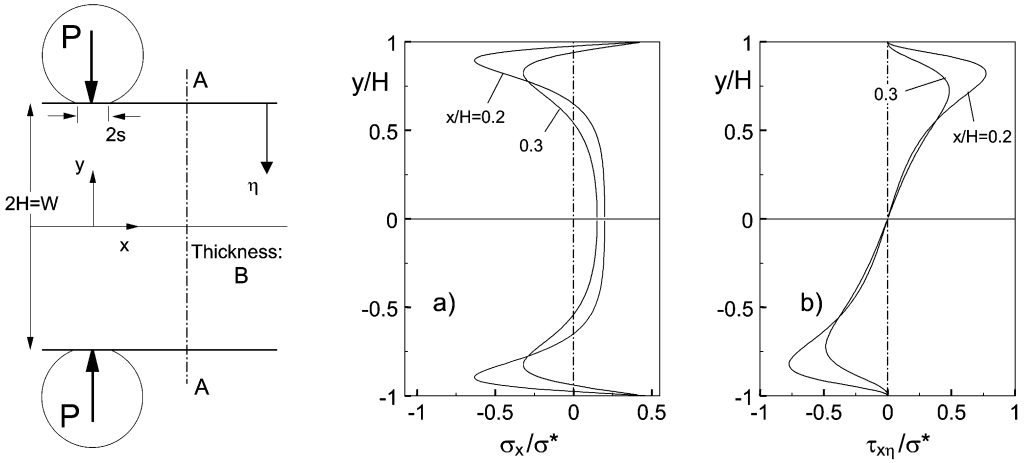

Fig. 4. (a) Geometric data for a bar loaded by two opposed cylinders, (b) stress normal to cross-section AA, (c) shear stress in cross-section AA.

$$K_{II} = \int_0^a h_{II}(\eta, a)\tau_{xy}(\eta)\mathrm{d}\eta \tag{23}$$

with the weight functions h_I for mode-I and h_{II} for mode-II loading and the distance η from the surface.

The results obtained with the weight function solutions given in Ref. 10 are plotted in Fig. 5a and b. From this representation, it is obvious that the mode-I stress intensity factors are positive first due to the tensile stresses near the free surface and then become negative at larger depths. In this case, at least partial crack closure must occur. The remaining stress intensity factor K_{II} is reduced by crack surface friction.

The effective stress intensity factor K_{eff}, combining K_I and K_{II}, was computed in Refs. 8 and 11 by a coplanar energy release rate criterion

$$K_{eff} = \begin{cases} \sqrt{K_I^2 + K_{II}^2} & \text{for} \quad K_I > 0 \\ K_{II} + \mu K_I & \text{for} \quad K_I < 0 \end{cases} \tag{24a}$$

with the coefficient μ chosen as $\mu = 0.5$.

As a further mixed-mode criterion, the empirical Richard formula[12] was applied. It provides the effective stress intensity factor[13]

$$K_{eff} = \begin{cases} \frac{1}{2}K_I + \sqrt{\frac{1}{4}K_I^2 + \frac{3}{2}K_{II}^2} & \text{for} \quad K_I > 0 \\ \sqrt{\frac{3}{2}}(K_{II} + \mu K_I) & \text{for} \quad K_I < 0 \end{cases} \tag{24b}$$

The resulting effective stress intensity factors are shown in Fig. 6. For the coplanar energy release rate criterion, the representation Fig. 6a shows that large cracks with $a/W > a^*/W$ (where $a^*/W \cong 0.015$) will predominantly fail near $x/s = 1$, whereas smaller cracks fail at a larger distance from the Hertzian contact zone. In the case of the Richard criterion (Fig. 6b), the same general behaviour is found, but now with a characteristic crack length of $a^*/W \cong 0.01$. For the cracks near $x/s = 1$ the slope in the log-log plot is for both criteria ≈ 1 and in case of larger distance $\approx 1/2$, i.e.

$$K_{eff,max} \propto \begin{cases} a & \text{for} \quad a/W > a^*/W \\ \sqrt{a} & \text{for} \quad a/W \leqslant a^*/W \end{cases} \tag{25}$$

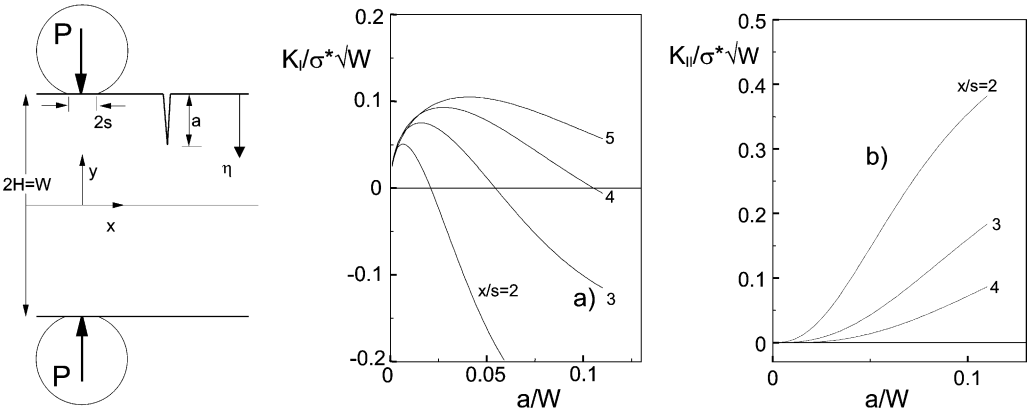

Fig. 5. Stress intensity factors for edge cracks: (a) mode-I and (b) mode-II stress intensity factor ($s/H = 0.1$).

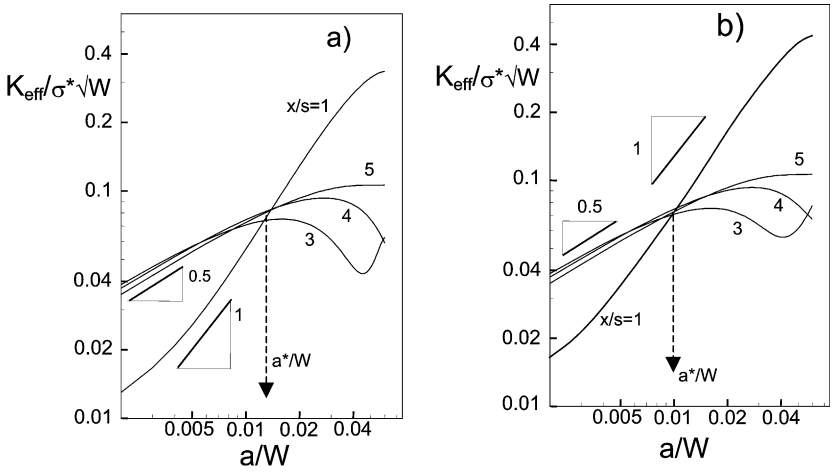

Fig. 6. Effective stress intensity factor K_{eff} for variably deep edge cracks as a function of the distance x from the contact centre: (a) computed with the coplanar energy release rate criterion, (b) with the Richard mixed-mode criterion.

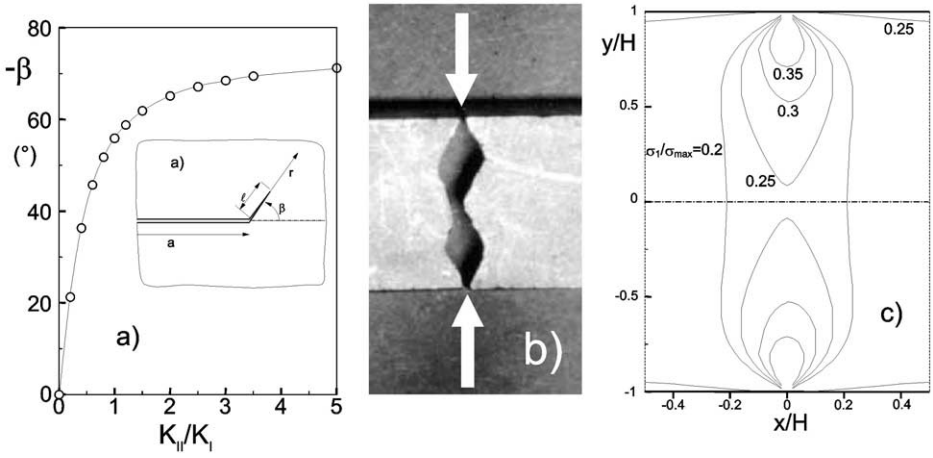

Fig. 7. (a) Kink angle,[13] (b) fracture paths under contact loading, (c) related first principal stress trajectories.

The considerations made before are sufficient to decide whether or not a given crack is able to start by spontaneous extension. Unfortunately, these results do not give any information on further crack growth phases, since the computations made before as well as the computations reported in Ref. 8 were based on the assumption of a coplanar crack extension.

Under this assumption, it would result from Fig. 6 that crack arrest is possible, because the effective stress intensity factors decrease again for large crack depths.

If a crack starts spontaneous propagation at an initial crack depth a, the crack abruptly changes its direction into the direction with a maximum mode-I contribution or, depending on the chosen criterion, into the direction with a maximum local energy release rate by generating a kink (Fig. 7a). In both cases, crack extension is roughly represented by the local condition $K_{II}=0$.

In a very good approximation, this condition is fulfilled for a crack shape coinciding with the maximum principal stress trajectory (Fig. 7b and c).

Extension along this curve ensures that the mode-II stress intensity factor disappears after a small amount of crack growth and the mode-I stress intensity factor increases monotonically. Therefore, it is not necessary to discuss crack arrest effects.

In Fig. 8 the ratio of the Weibull exponents for contact loading and bending is plotted versus the ratio $(K_{Ic}/\sigma_c)^2$ which for the bending strength is proportional to the initial crack size. It is obvious that for short cracks the Weibull exponents in both tests are identical, whereas for longer cracks lower exponents for the contact strengths are visible.

The change of the Weibull exponent is in agreement with the computations made before. If the asymptotic behaviour of the flaw size distribution can be described by a power law

$$f(a) \propto \frac{1}{a^r}, \tag{26}$$

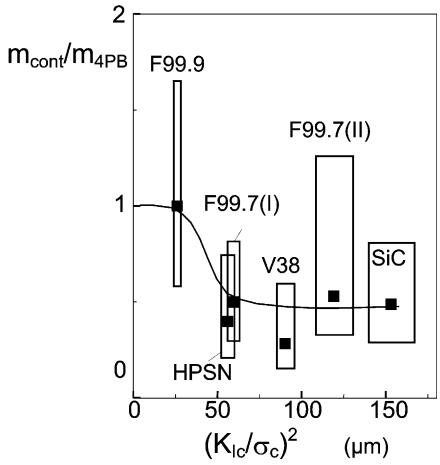

Fig. 8. Ratio of Weibull exponents for contact and bending strength versus the initial crack size $a \propto (K_{Ic}/\sigma_c)^2$.

the related strength distribution $F(\sigma_c)$ reads

$$F(\sigma_c) = 1 - \exp\left[-zS\left(\frac{a_0}{a}\right)^{r-1}\right] \tag{27}$$

where z is the number of cracks per surface unit and S the surface of the component. Introducing the relation between crack size a and strength σ_c in the form of

$$a \propto \sigma_c^{-p} \tag{28}$$

into (27) yields

$$F(\sigma_c) = 1 - \exp\left[-\left(\frac{\sigma_c}{\sigma_0}\right)^m\right] \tag{29}$$

with the characteristic strength σ_0 and

$$m = p(r-1) \tag{30}$$

As a consequence of Eq. (25), we obtain the usual value of $p=2$ for the failure of *short cracks* and for cracks in the absence of strong stress gradients

$$m_{short} = m_{4PB} = 2(r-1). \tag{31a}$$

For *longer cracks* with the failure being directly at the end of the Hertzian contact

$$m_{\text{long}} = r - 1, \tag{31b}$$

i.e. the ratio of the Weibull exponents of contact and bending strength is expected to be 1 for short cracks and $\frac{1}{2}$ for longer cracks.

5. Summary

The flaw size distribution is responsible for the large scatter in strength of ceramic materials and for effect of the size of a component on the strength. Under moderate stress gradients the Weibull parameter m representing the scatter of the strength distribution is independent on any chosen loading situation. In the case of ceramics under high stress gradients m differs from that for moderate stress gradients. This is illustrated for a contact loading test, where most ceramics strengths showed strongly reduced Weibull exponents compared with those from four-point bending tests. This effect is interpreted as the consequence of non-homogeneous stresses with steep gradients.

Acknowledgements

The authors thank the Deutsche Forschungsgemeinschaft DFG for financing part of this work within the SFB 483.

References

1. Jayatilaka, A., De, S. and Trustrum, K., Statistical approach to brittle fracture. *J. Mat. Sci.*, 1977, **12**, 1426–1430.
2. Davies, D. G. S., The statistical approach to engineering design in ceramics. *Proc. Br. Ceram. Soc.*, 1973, **22**, 429–452.
3. Bansal, G. H., Duckworth, W. H. and Niesz, D. E., Strength-size relations in ceramics. *J. Am. Ceram. Soc.*, 1976, **59**, 472–478.
4. Evans, A. G., A general approach for the statistical analysis of multi-axial fracture. *J. Am. Ceram. Soc.*, 1978, **61**, 302–308.
5. Batdorf, S. B. and Heinisch, H. L., Weakest link theory reformulated for arbitrary fracture criterion. *J. Am. Ceram. Soc.*, 1978, **61**, 355–358.
6. Lemon, J., Statistical approaches to failure for ceramic reliability assessment. *J. Am. Ceram. Soc.*, 1988, **71**, 106–112.
7. Fett, T., Munz, D. and Thun, G., Test devices for strength measurements of bars under contact loading. *J Testing and Evaluation*, 2001, **29**, 1–10.
8. Fett, T. and Munz, D., Influence of stress gradients on failure in contact strength tests with cylinder loading. *Engng. Fract. Mech.*, 2002, **69**, 1353–1361.
9. Munz, D. and Fett, T., *CERAMICS, Failure, Material Selection, Design*. Springer-Verlag, März, 1999.
10. Fett, T. and Munz, D., *Stress Intensity Factors and Weight Functions*. Computational Mechanics Publications, Southampton, UK, 1997.
11. Fett, T., Mixed-mode stress intensity factors for partially opened cracks. *Int. J. Fract.*, 2001, **111**, L67–L72.
12. Richard, H. A., *Prediction of Fracture of Cracks Subjected to Combined Tensile and Shear Loads*. VDI Research Report 631/85, 1985, Düsseldorf, Germany (in German).
13. Fett, T. and Munz, D., Kinked cracks and Richard fracture criterion. *Int. J. Fract.*, 2002, **115**, L69–L73.